Gold Nanoparticle-electrodeposited Electrodes Used for *p*-Nitrophenol Detection in Acidic Media: Effect of Electrodeposition Parameters on Particle Density, Size Distribution, and Electrode Performance

Ying-Yao Tang and Po-Yu Chen*
Department of Medicinal and Applied Chemistry, Kaohsiung Medical University, Kaohsiung City 807, Taiwan, R.O.C.

Received January 31, 2011; Accepted April 14, 2011; Published Online April 28, 2011

Para-nitrophenol (*p*-NP) was detected using gold nanoparticle-electrodeposited indium tinoxide electrodes (AuNP-ITO) or AuNP-electrodeposited screen printing carbon electrodes (AuNP-SPC) in acidic media. AuNPs were formed by potential-sweeping electrodeposition from the solution containing Na_2SO_4, H_2SO_4, and $HAuCl_4 \cdot 3H_2O$. The effect of electrodeposition parameters, such as the cycling number of potential scan, the cathodic switching potential, and the scan rate, on density and size distribution of AuNPs was studied. It was found that the particle density and the size distribution of the AuNPs had a crucial effect on the electrode activity to *p*-NP reduction. A AuNP-electrodeposited electrode with appropriate size, narrow distribution, and high density of AuNPs shows the best activity to *p*-NP reduction. *p*-NP was detected by hydrodynamic chronoamperometry at –0.2 V and the dependence of the steady state current taken from the amperometric transient on concentration of *p*-NP was linear from 1.0×10^{-7} M to 3.15×10^{-4} M with a regression coefficient of 0.9995. The detection limit was 9.8×10^{-8} M (13.7 ppb) ($\sigma = 3$).

Keywords: Gold nanoparticle; *p*-Nitrophenol; Electrodeposition; Indium tin oxide electrode; Modified electrode.

INTRODUCTION

Compounds of substituted phenols, e.g. nitrophenols (NPs), are widely employed or produced in many industrial processes including pesticides, pharmaceuticals, preservatives, and etc. Many of them are toxic, accumulative, carcinogenic, and environmentally persistent.[1-3] *p*-Nitrophenol (4-nitrophenol; *p*-NP or 4-NP) is one of the severely toxic substituted phenols. Therefore, to develop a fast and sensitive method to detect *p*-NP in industrial waste waters, natural waters, and drinking waters is great important. *p*-NP is a toxic derivative related to several organophosphorous pesticides such as methyl-parathion, ethyl-parathion, fenitrothion, and etc. The US Environmental Protection Agency (EPA), therefore, has provided the allowed limit of *p*-NP in drinking water at 60 ppb (~ 0.43 μM).

Electrochemical detection of *p*-NP is important and attractive because electrochemical devices are always compact and electrochemical analysis usually provides high sensitivity. *p*-NP has been widely detected by using a variety of electrodes, including graphite[4-6] and glassy carbon (GC) electrodes,[7] inorganic-organic hybrid-modified Pt electrode,[8] boron doped diamond (BDD) electrode,[9] single-wall carbon nanotube (SWCNT)-coated GC electrode,[10] zeolite-modified carbon paste electrode,[11] silver-amalgam electrode,[12] bismuth-modified GC electrode,[13] and poly(Ni-(protoporphyrin IX))-modified GC electrode.[14] Some of these electrodes were employed as detectors for HPLC that isolated *p*-NP from its isomers.

Gold nanoparticle (AuNP) has been extensively used for a lot of application, including the AuNP-modified electrodes.[15] AuNP-modified electrodes can be prepared by potential-step or pulse-potential electrodeposition and the control of particle density and size distribution achieved by adjusting the electrodeposition parameters was discussed.[16] Reversely, electrodeposition of AuNPs was rarely achieved by potential-sweeping electrodeposition

Special issue for the nanotechnology-related analytical chemistry

* Corresponding author. Tel: +886 7 3121101 ext. 2587; Fax: +886 7 3125339; E-mail: pyc@kmu.edu.tw

and the influence of electrodeposition parameters on particle density and size distribution was not investigated.[17] AuNP-modified electrodes usually exhibit a unique electrocatalytic behavior or high sensitivity. Surprisingly, no AuNP-modified electrode has been used for the detection of *p*-NP or its isomers except that the gold nanoporous electrode prepared by simple dealloying process was recently employed to detect *p*-NP.[18] This electrode demonstrates a very unusual selectivity to *p*-NP from its isomers, *o*-NP and *m*-NP. Based on our previous study, AuNPs could be easily formed on indium tin oxide-coated glass electrode (ITO) by potential-sweeping and potential-step electrodeposition, respectively.[19] Smaller AuNPs with higher particle density were obtained by potential-sweeping method. The AuNP-modified electrode significantly improved the sensitivity on the detection of Cr(VI). It is, therefore, interesting to know whether this AuNP-electrodeposited ITO electrode (AuNP-ITO) has a similar effect on the electrochemical detection of *p*-NP.

In this study, the AuNP-ITO and AuNP-electrodeposited screen printing carbon (AuNP-SPC) electrodes prepared by potential-sweeping electrodeposition were employed to detect *p*-NP in acidic media. In neutral media, these electrodes were still workable but an acidic environment is more beneficial for *p*-NP reduction because protons are essential in the reduction of *p*-NP. The effect of the electrodeposition parameters, such as the cycling number of potential scan, the cathodic switching potential, and the scan rate of potential, on the particle density and the size distribution of the AuNPs was carefully studied because density and distribution always have a crucial effect on the electrode performance.[20] Scanning electron microscope (SEM) was used to obtain the surface images of the AuNP-ITO electrodes and these SEM micrographs were analyzed by image software in order to calculate the number and size distribution of the obtained AuNPs in a particular area. An X-ray thin-film diffractometer (XRD) was employed to analyze the crystalline structure of the AuNPs in order to know whether a favored phase existed in the obtained AuNPs.

RESULTS AND DISCUSSION

Voltammetric study of Au(III) and *p*-nitrophenol

Before electrodeposition of AuNPs would be carried out, the voltammetric behavior of Au(III) must be studied at an ITO electrode in the solution containing 0.01 M Na_2SO_4, 0.01 M H_2SO_4, and 1 mM $HAu(III)Cl_4 \cdot 3H_2O$. This solution was used because AuNPs with high density and small size could be easily obtained by electrodeposition. Fig. 1 shows the continuous cyclic voltammograms (CVs) recorded at an ITO electrode in the Au(III) solution. The applied potential was initially scanned from +1.5 V (vs. Ag/AgCl) in the negative direction and then reversed at –0.6 V. At the first cycle, a broad reduction wave was observed near 0.0 V, indicating the reduction of Au(III) to Au(0) deposited on the electrode surface. A current loop was observed at the subsequent reverse scan and a sharp oxidation peak was observed near 1.0 V. This oxidation reaction should result from the oxides formation of the deposited Au formed during the cathodic half-cycle. In the following second to seventh cycle, the reduction wave of Au(III) disappeared. Actually, it shifted to a more positive potential where the reduction of Au oxides formed during the anodic scans simultaneously occurred. In addition, no current loop was observed after the second cycle. This behavior indicated that nucleation processes and higher overpotential were essential for electrodeposition of Au at a fresh ITO electrode. A much lower overpotential was needed for Au electrodeposition after Au particles have been formed on the electrode surface at the first cycle. Except for the first cycle, the current response increased with the number of potential scan, indicating the formation and growth of Au particles. The aforementioned behavior was

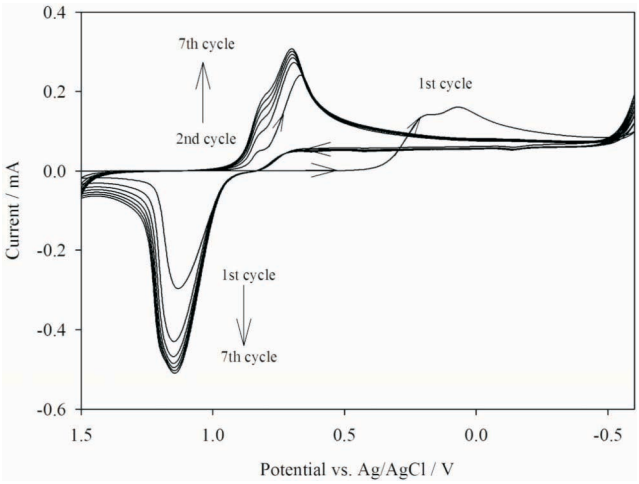

Fig. 1. Continuous cyclic voltammograms recorded at an ITO electrode in the solution containing 0.01 M Na_2SO_4, 0.01 M H_2SO_4, and 1 mM $HAuCl_4 \cdot 3H_2O$. Scan rate: 50 mVs^{-1}.

also observed at a SPC electrode (data not shown).

The voltammetric behavior of *p*-NP was studied at three different electrodes to know whether a AuNP-modified electrode could provide any benefit to the electrochemical detection of *p*-NP. Fig. 2 demonstrates the first cycles of three CVs recorded at AuNP-ITO (AuNP potential-sweeping electrodeposition-coated ITO electrode), Au-ITO (Au sputtering deposition-coated ITO electrode), and bare ITO electrodes, respectively. Apparently, the bare ITO electrode showed a high overpotential on the reduction of *p*-NP. A coating of gold on ITO electrode obviously reduced the overpotential necessary for *p*-NP reduction, especially for the AuNP-ITO electrode in which *p*-NP was reduced at the most positive potential and a peak-like reduction signal was observed. Fig. 2 indicates that AuNPs really improved the electrode performance in the respects of the overpotential reducing and the reaction current enhancing. In general, the particle density and the size distribution of AuNPs are crucial to the electrode performance and the electrodeposition parameters determine them. Therefore, it is important and essential to find out what the optimum conditions of AuNP electrodeposition are for *p*-NP detection.

Electrodeposition of AuNPs—effects of scan cycles, switching potentials, and potential scan rates

As aforementioned in the experimental section, AuNPs were formed by potential-sweeping electrodeposition because more appropriate size and higher particle density of AuNPs could be obtained. For potential-sweeping electrodeposition, the adjustable parameters were the cycle number of potential scan, the cathodic switching potential (the anodic switching potential was fixed at +1.5 V), and the rate of potential scan. The cathodic peak current of *p*-NP (please see Fig. 2) observed at AuNP-ITO or AuNP-SPC electrodes was used as the criterion to assess the performance of the AuNP-electrodeposited electrodes that were formed by employing different potential-sweeping conditions. When the cathodic switching potential and the scan rate for the potential-sweeping electrodeposition were fixed at –0.6 V and 80 mVs^{-1}, respectively, the experimental data indicated that the cathodic peak current of *p*-NP increased with increasing the cycle number of potential scan. The reaction current of *p*-NP reached a plateau after 7 cycles because individual AuNPs started to aggregate together. The tendency observed at the AuNP-SPC electrode was almost identical to the AuNP-ITO electrode except that the reduction current of *p*-NP was higher at the AuNP-ITO electrode. Based on shortening the time necessary for electrodeposition and improving the reduction peak current of *p*-NP, the cycle number of potential scan for electrodeposition was determined to be 7 in the following experiments.

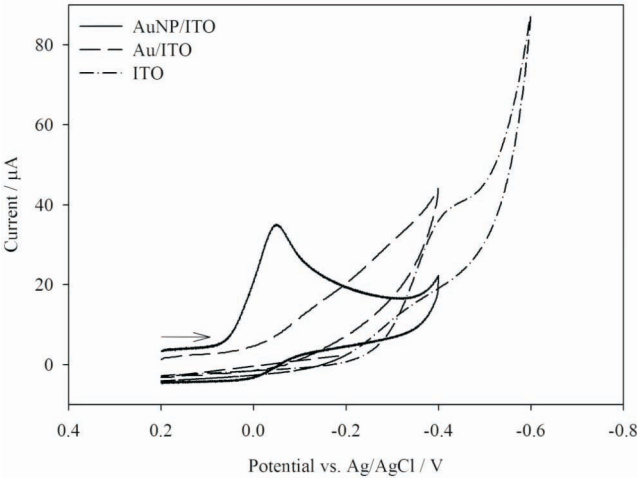

Fig. 2. Cyclic voltammograms recorded at three different electrodes in the deaerated solution containing 0.1 M $HClO_4$, 1 mM $NaClO_4$, and 50 μM *p*-NP. Scan rate: 50 mVs^{-1}.

The effect of the cathodic switching potential (0.0 V ~ –0.6 V) employed for the AuNP potential-sweeping electrodeposition on the cathodic peak current of *p*-NP was studied and the experimental result indicated that a higher reductive peak current of *p*-NP was observed when a more negative switching potential was used. In this experiment, the scan rate and the cycle number were fixed at 80 (mVs^{-1}) and 7 (cycles). This correlation was expectable because more AuNPs should be formed on the electrode surface when a more negative switching potential was employed. Two electrodes (AuNP-ITO and AuNP-SPC) demonstrated a similar behavior. The switching potentials more negative than –0.6 V were not studied because severe hydrogen evolution was encountered. Based on the experimental result, the cathodic switching potential at –0.6 V was employed for the following electrodeposition.

Fig. 3 indicates that the cathodic peak current of *p*-NP decreased with increasing the scan rate of potential for AuNP electrodeposition. Therefore, the AuNP-electrodeposited electrodes prepared by setting the scan rate at 50 mVs^{-1} showed the highest response toward the *p*-NP reduc-

tion when 7 cycles of potential scan and –0.6 V of cathodic switching potential were used for the electrodeposition. If a slower scan rate (ex., 20 mVs^{-1}) is used for the electrodeposition of AuNPs, only regular Au-coated electrodes were obtained. The electrode surface was golden rather than red (the characteristic color of AuNP). The tendency observed at AuNP-ITO and AuNP-SPC electrodes was similar (Fig. 3) except that higher currents were observed at AuNP-ITO.

In conclusion, the ultimate conditions of electrodeposition were determined according to the aforementioned experimental results; 7 cycles of potential scan, –0.6 V of cathodic switching potential, and 50 mVs^{-1} of potential scan rate, respectively. Formation of AuNPs was carried out by using the ultimate conditions of electrodeposition on ITO and SPC electrodes. These two electrodes were used to detect 50 μM *p*-NP for 30 times by using cyclic voltammetry in the solution containing 0.1 M $HClO_4$ and 1 mM $NaClO_4$ to understand the short-term stability of the AuNP-electrodeposited electrodes. The ratios of the cathodic peak currents of *p*-NP (i_p) divided by the maximum cathodic peak current of *p*-NP ($i_{p,max}$) selected from the 30 detections are shown in Fig. 4. It can be found that the AuNP-ITO electrode showed a better stability (R.S.D = 0.65%) than the AuNP-SPC electrode (R.S.D = 2.7%).

It is very interesting and important to know why the AuNP-coated electrodes prepared from different electrodepositing conditions showed such enormous variations on *p*-NP reduction current. Four selected AuNP-ITO electrodes prepared from different conditions were characterized with SEM and the SEM micrographs were analyzed with ImageJ software to obtain the information about particle size distribution. ITO was used for SEM observation because ITO electrode exhibited a very smooth surface that is essential for a precise image analysis. The SEM micrographs of the four AuNP-ITO electrodes and the analytical results are illustrated in Fig. 5. The *x*-axis indicates the diameter of AuNPs in an interval of 20 (e.g., 20 means > 1 but ≤20, 40 means > 21 but ≤40, and so on) and the *y*-axis represents the number of AuNPs in each interval at the *x*-axis. Fig. 5a shows the analytical result of particle size distribution for the AuNP-ITO where AuNPs were formed using the ultimate electrodeposition condition. The inset of Fig. 5a shows the SEM micrograph of this AuNP-ITO electrode. As can be seen, the AuNP-ITO prepared from the ultimate electrodeposition parameters exhibited a narrower size distribution of AuNPs (size distribution: 43.3 ± 27.5 nm) and more particles in the same image size (698 particles). The electrodeposition parameters employed for the sample shown in Fig. 5a were used to prepare another

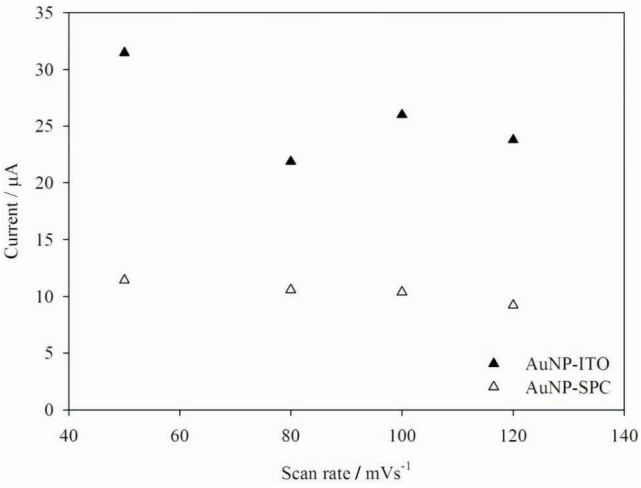

Fig. 3. The dependence of *p*-NP (50 μM) reductive peak currents (obtained from CVs) recorded at AuNP-ITO and AuNP-SPC in the deaerated solution of 0.1 M $HClO_4$ and 1 mM $NaClO_4$ on the scan rate for electrodeposition. Electrodeposition parameters of AuNPs: cathodic reversed potential: –0.6 V, cycle number: 7.

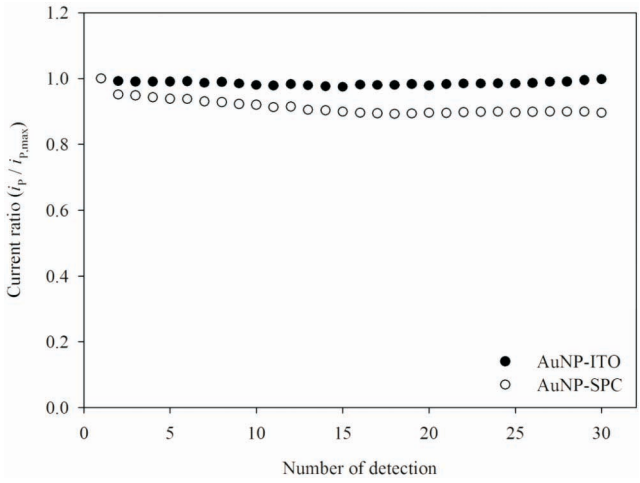

Fig. 4. The short-term stability of AuNP-ITO and AuNP-SPC on *p*-NP reduction. i_p (peak current of *p*-NP reduction) / $i_{p,max}$ (maximum peak current of *p*-NP reduction) for the 30 detections of 50 μM *p*-NP in the deaerated solution of 0.1 M $HClO_4$ and 1 mM $NaClO_4$ was shown. AuNPs were electrodeposited using the ultimate parameters; cathodic switching potential: –0.6 V, scan rate: 50 mVs^{-1}, cycle number: 7.

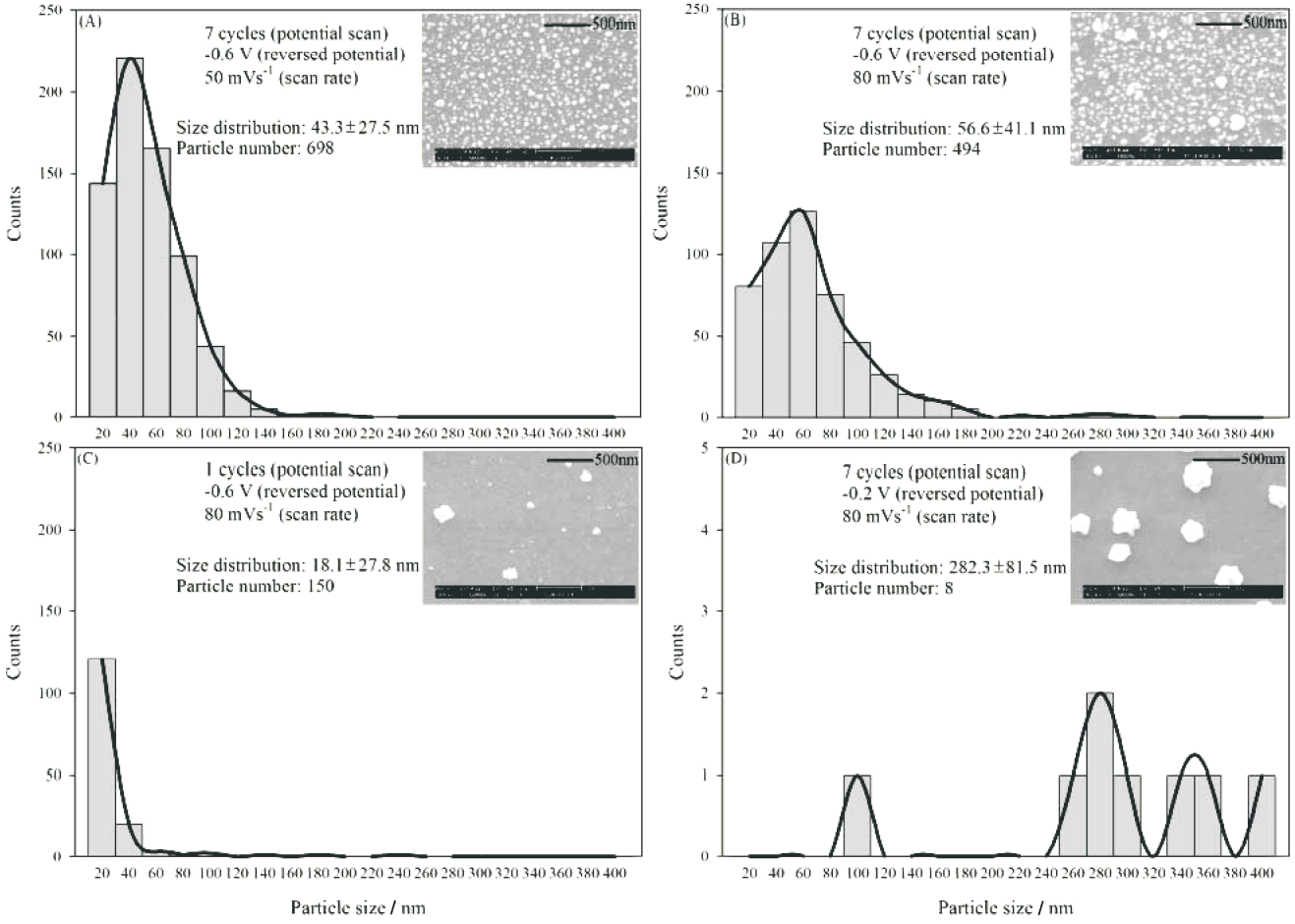

Fig. 5. SEM micrographs and particle size histograms of AuNPs electrodeposited on ITO electrodes. The electrodeposition parameters, size distribution, and particle number calculated from each micrograph are indicated in individual plot.

AuNP-ITO (Fig. 5b) except that the scan rate was 80 mVs^{-1} rather than 50 mVs^{-1}. By simply adjusting the scan rate to 80 mVs^{-1}, the size distribution of AuNPs significantly changed (Fig. 5b); the average particle size became bigger and the size distribution became more divergent (size distribution: = 56.6 ± 41.1 nm). In addition, fewer particles (494 particles) were obtained if increasing the scan rate. The inset of Fig. 5b indicates that there were several apparent aggregates of AuNPs and the particles did not equally disperse on the electrode surface, compared with the inset of Fig. 5a. When the electrodepositing parameters for the sample of Fig. 5b were employed but only one cycle of potential scan was performed to prepare the AuNP-ITO (Fig. 5c), this electrode demonstrated a much smaller cathodic peak current of *p*-NP than the electrode shown in Fig. 5b. Fig. 5c indicates that this electrode possessed very few particles (150 particles) and the smallest average particle size (size distribution: = 18.1 nm ± 27.8). The electrodeposition parameters used for the sample in Fig. 5b were employed to prepare a AuNP-ITO electrode but the cathodic switching potential of –0.2 V was used instead of –0.6 V. The SEM micrograph and the analytical data of this AuNP-ITO were shown in Fig. 5d. It can be found that cathodic switching potential has a crucial effect on the number and size of the AuNPs (size distribution: = 282.3 ± 81.5 nm; 8 particles). An insufficiently negative potential evidently could not provide sufficient free energy for the formation of nuclides. According to the CV shown in Fig. 1, electrodeposition of AuNPs needs a high overpotential on a fresh ITO surface. Therefore, only few nuclides of Au were formed, if the switching potential is too positive. Gold only grew on the existing nuclides, resulting in these few and big particles

on the same image area of the ITO surface.

Based on this analysis, a conclusion could be made that the cathodic switching potential and the cycle number of potential scan determined the particle density and size distribution of AuNPs. This behavior is reasonable because a more negative switching potential definitely can provide higher energy for nuclide formation, leading to a higher density of nuclides. More cycles of potential scan also can produce more nuclides for growing. Actually, the nucleation mechanism of Au electrodeposition in the solution has been determined. A 3D progressive nucleation was involved in the electrodeposition of AuNPs (data not shown). It could explain why the number of nuclides could be increased by increasing the cycle number of potential scan. On the other hand, the scan rate of potential seemed to determine the degree of size distribution. A moderate scan rate (in this study, 50 mVs^{-1}) leads to a narrower distribution of AuNPs on the electrode surface. Again, it could be concluded that the AuNP-ITO electrode with the highest particle density, the moderate particle size, and the narrower distribution of particles showed the best electrode activity to *p*-NP reduction.

In order to confirm that the electrode performance is determined by the size effect from AuNPs rather than the effect of preferred crystal phases, a AuNP-ITO prepared by electrodeposition using the ultimate parameters and a Au-ITO (gold sputtering deposition-coated ITO electrode) were analyzed with a thin-film XRD. The X-ray diffraction patterns of these two electrodes and a bare ITO electrode were shown in Fig. 6. The characteristic signals of Au were denoted on the figure. As can be seen, the distribution of crystal phases observed at the AuNP-ITO electrode was identical to that observed at the Au-ITO electrode; no preferred crystal phase was found at the AuNP-ITO. This result supported that the electrode activity to *p*-NP reduction was determined by the particle density and size distribution of AuNPs. Based on Fig. 6 and the Scherrer's equation, the crystal size of Au coating on the AuNP-ITO and the Au-ITO electrodes were determined to be 16.1 nm and 11.8 nm, respectively. This result supported that moderate particle size of AuNPs contributed to the better electrode performance (Fig. 2); too small or too big AuNPs degraded the electrode activity.

In the aforementioned experiments, ITO electrodes were employed because a very smooth surface was essential for the analysis of particle size distribution. However, AuNP-SPC electrodes were employed for *p*-NP detection based on the consideration of convenience. Because the AuNP-SPC electrode always shows a similar behavior as observed at the AuNP-ITO electrode, the conclusion made for the AuNP-ITO electrode is reasonable for the AuNP-SPC electrode.

Calibration curve of *p*-NP

The AuNP-SPC electrode prepared by employing the ultimate electrodepositing parameters was used to detect *p*-NP in acidic media (0.1 M $HClO_4$ + 1 mM $NaClO_4$) by hydrodynamic chronoamperometry. The acidic media was firmly stirred by a magnetic stirrer to obtain limiting current when amperometric measurements were carried out. A constant potential of –0.2 V was applied at the AuNP-SPC electrode immersed in the firmly stirred solution. The standard solution of *p*-NP was successively injected and a limiting current was measured after each injection (the inset of Fig. 7). The value of the limiting current was taken to establish the calibration curve as shown in Fig. 7. The dependence of the limiting current on the concentration of *p*-NP was linear from 0.1 μM to 315 μM with a slope of 0.2886 $\mu A \mu M^{-1}$ and a regression coefficient of 0.9995. The detection limit was 0.098 μM ($\sigma = 3$). A recovery test was carried

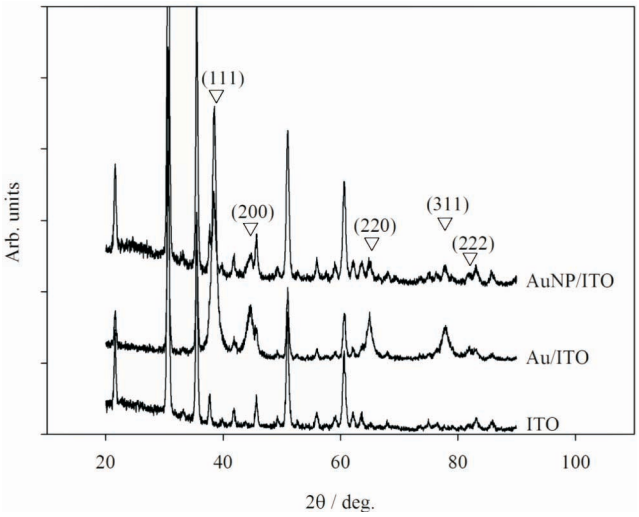

Fig. 6. Thin film XRD patterns of ITO, Au-ITO (gold sputtering deposition-coated ITO electrode), and AuNP-ITO electrodes. AuNP-ITO was prepared by potential-sweeping electrodeposition in which the ultimate parameters were employed.

Table 1. Determination of *p*-NP in several water samples

	Deionized water	Tap water	Ground water
Detected value, original (μM)	ND	ND	ND
p-nitrophenol added (μM)	4.99	4.99	9.99
p-nitrophenol found after addition (μM)	4.96	4.86	9.98
Recovery (%)	99 ± 3.42	97 ± 3.53	100 ± 14.03

out in deionized water containing 0.1 M $HClO_4$ and 1 mM $NaClO_4$; the result is shown in Table 1.

Interferences

Five inorganic anions (SO_4^{2-}, NO_3^-, CO_3^{2-}, PO_4^{3-}, and Cl^-), six metal ions (Zn^{2+}, Ni^{2+}, Fe^{2+}, Co^{2+}, Cu^{2+}, and Hg^{2+}), and two organic compounds (phenol and aniline) were individually introduced (20 ~ 800× excess over *p*-NP) into the acidic media (0.1 M $HClO_4$ + 1 mM $NaClO_4$) containing 50 μM *p*-NP in order to know their influence on the reductive peak current of *p*-NP recorded at AuNP-SPC. The reductive peak current ratios (i_{ratio}) of 50 μM *p*-NP in the presence and absence of interfering substances are shown in Fig. 8. The i_{ratio} of 50 μM *p*-NP in the absence of interfering substances was defined as 1.0. As can be seen in Fig. 8, the i_{ratio} varied from 0.91 to 1.09. Cu^{2+} and Hg^{2+} showed very serious interference on *p*-NP detection because these two ions were reduced to metals at the potentials close to or more positive to the reduction potential of *p*-NP. Ion-exchange resin, therefore, had to be employed to exchange these two ions by Na^+ ions. Otherwise the reductive peak current of *p*-NP was significantly altered. Although ion-exchange was used as the pretreatment method, Hg^{2+} still showed serious interference when its concentration in the original solution was 20× excess over *p*-NP (i_{ratio} = 1.09, Fig. 8). By the way, it is very unfortunate that *o*-NP, *m*-NP, and nitrobenzene have serious interference on the detection of *p*-NP because all three compounds show overlapped reductive waves with that of *p*-NP at the AuNP-modified electrode. It is, therefore, have to separate the three compounds by an appropriate method if the water samples contain these three interfering compounds.

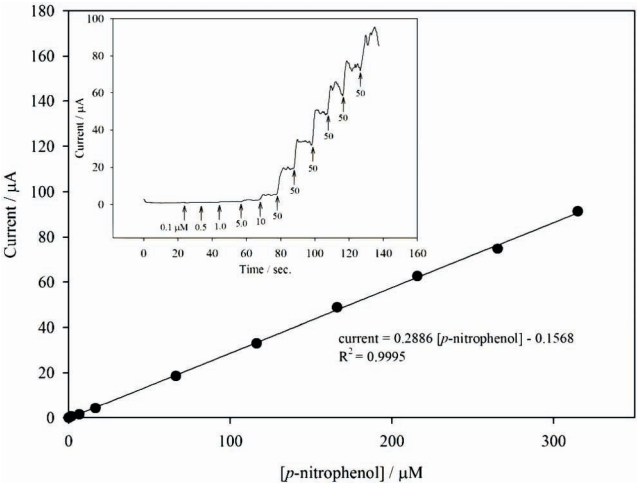

Fig. 7. The calibration curve of *p*-NP. It was constructed by using the limiting current response taken from the current transient that is shown in the inset. Detection potential: –0.2 V.

Determination of *p*-NP in water samples

The analytical application of AuNP-SPC electrode was demonstrated by using it to determine the concentration of *p*-NP in tap water and in ground water, respectively. In the original water samples, no *p*-NP was detected. However, it must be emphasized that the content of *p*-NP in the original samples might be lower than our detection limit.

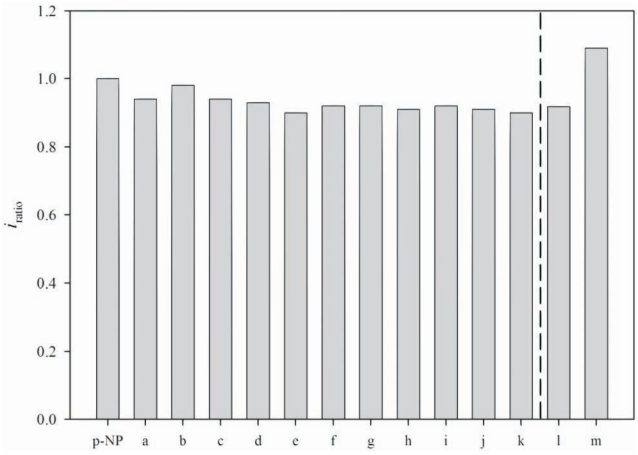

Fig. 8. Cathodic peak current ratio of 50 μM *p*-NP at the AuNP-SPC electrode in the presence of (a) SO_4^{2-} (800×), (b) NO_3^- (800×), (c) CO_3^{2-} (800×), (d) PO_4^{3-} (800×), (e) Cl^- (800×), (f) Zn^{2+} (300×), (g) Ni^{2+} (800×), (h) Fe^{2+} (300×), (i) Co^{2+} (800×), (j) phenol (217×), (k) aniline (163×), (l) Cu^{2+} (638×) , (m) Hg^{2+} (20×). The number in the parenthesis indicates the concentration excess over *p*-NP for the interfering substances. (l) and (m) were pretreated using the ion-exchange process before introducing them into the solution containing *p*-NP.

Therefore, a recovery test was carried out by introducing a known concentration of *p*-NP into the water samples to confirm the feasibility of this entire method. For each sample, hydrodynamic chronoamperometry was performed to acquire the electrochemical signals. The experimental results were collected in Table 1. Good recovery ratios were obtained, indicating that this analytical method may be appropriate to be applied in the detection of *p*-NP in tap water and ground water. It has to emphasize that 0.1 M $HClO_4$ and 1 mM $NaClO_4$ were introduced into each water sample.

CONCLUSIONS

Particle density and size distribution of AuNPs always have a crucial role on the activity of AuNP-modified electrodes. In this study, the AuNP-modified electrode with a higher particle density, a moderate particle size, and a narrower size distribution of AuNPs showed the best activity to *p*-NP reduction. In potential-sweeping electrodeposition of AuNPs, the desired density, size, and distribution of AuNPs can be achieved by simply adjusting the electrochemical parameters, including the cycle number of potential scan, the cathodic switching potential, and the scan rate. Based on this study, a more precise method is probable to be developed to prepare a AuNP-modified electrode with higher activity for electroanalytical purpose.

EXPERIMENTAL

Apparatus and chemicals

All electrochemical experiments were performed with a CHI 621A electrochemical analyzer (CH Instruments, Inc.) in conjunction with a model C-2 cell stand (Bioanalytical Systems; BAS). A three-electrode cell was employed. The cell consisted of an indium tin oxide-coated glass electrode (ITO) or a disposable screen printing carbon electrode (SPC; provided from Zensor R&D, Taiwan) upon which gold nanoparticles (AuNPs) were formed by electrodeposition, a Ag/AgCl (in saturated NaCl) reference electrode, and a spiral platinum counter electrode. The ITO electrodes were obtained by cutting a large piece of ITO into smaller pieces with an individual area of 0.6 × 1.2 cm^2. They were washed supersonically in acetone, and then in deionized water, and dried in a vacuum oven at room temperature before experiments would be carried out. The conducting area of each ITO electrode was restricted in 0.6 × 0.5 cm^2 by wrapping the unnecessary area with Teflon tape. The SPC electrode with a geometric surface area of 0.196 cm^2 was used as purchased. A Philips XL-40FEG field emission scanning electron microscope (FESEM) coupled with an energy dispersive spectrometer (EDS) was used to investigate the surface morphologies and the elemental compositions of the AuNP coatings. The crystalline structures of the AuNPs were analyzed with a Rigaku D/MAX2500 multipurpose X-ray thin-film diffractometer (XRD).

Sulfuric acid (SHOWA), perchloric acid (SHOWA), sodium sulfate (TEDIA), sodium perchlorate (SHOWA), hydrogen tetrachloroaurate(III) trihydrate (ACROS), and *p*-nitrophenol (*p*-NP) (ACROS) were used as received without further purification. Ion-exchange resin (Amberlite IR-120(Plus)) was purchased from Aldrich and used to displace Hg^{2+} and Cu^{2+} in aqueous samples by Na^+ ions. All aqueous solutions were prepared using deionized water purified by the Milli-Q Gradient system (Millipore).

Electrodeposition of gold nanoparticles

An aqueous solution containing 0.01 M Na_2SO_4, 0.01 M H_2SO_4, and 1 mM $HAuCl_4 \cdot 3H_2O$ was employed for electrodeposition of AuNPs at ITO or SPC electrodes (AuNP-ITO or AuNP-SPC). Based on our previous study,[19] smaller AuNPs with higher particle density could be obtained by potential-sweeping electrodeposition. Therefore, only potential-sweeping electrodeposition was used to form AuNPs in this study and no effort was devoted on improving the potential-step electrodeposition. Potential-sweeping electrodeposition was carried out by using cyclic voltammetry. The effect of cyclic voltammetric parameters, such as the number of potential scan (1 ~ 9 cycles), the cathodic switching potential (0 ~ –0.6 V), and the potential scan rate (50 ~ 120 mVs^{-1}), on the particle density and the size distribution of the AuNPs was carefully studied. The optimal parameters for electrodeposition of AuNPs were determined as 7 cycles of potential scan, –0.6 V of cathodic switching potential, and 50 mVs^{-1} of potential scan rate because the highest response of *p*-NP was observed at this AuNP-modified electrode. The SEM micrographs of several selected AuNP-ITO electrodes were analyzed with ImageJ (version 1.42) software to know the distribution of particle size.

ACKNOWLEDGEMENTS

This work is supported by the National Science Council of Taiwan (NSC98-2113-M-037-007-MY3). The service supplied from the Instrument Center of National

Cheng Kung University is sincerely appreciated.

REFERENCES

1. Penalver, A.; Pocurull, E.; Borrull, F.; Marce, R. M. *J. Chromatogr., A* **2001**, *953*, 79.
2. Nasr, B.; Abdellatif, G. *J. Electrochem. Soc.* **2005**, *152*, D113.
3. Cong, Y.; Wu, Z.; Ye, Q.; Tan, T.; Zhejiang, J. *Science* **2004**, *5*, 180.
4. Bebeselea, A.; Manea, F.; Burtica, G.; Nagy, L.; Nagy, G. *Talanta* **2010**, *80*, 1068.
5. Rueda, M. E.; Sarabia, L. A.; Herrero, A.; Ortiz, M. C. *Anal. Chim. Acta* **2001**, *446*, 269.
6. Galeano-Diaz, T.; Guiberteau-Cabanillas, A.; Mora-Diez, N.; Parrilla-Vazquez, P.; Salinas-Lopez, F. *J. Agric. Food Chem.* **2000**, *48*, 4508.
7. Honeychurch, K. C.; Hart, J. P. *Electroanalysis* **2007**, *19*, 2176.
8. Lupu, S.; Lete, C.; Marin, M.; Totir, N.; Balaure, P. C. *Electrochim. Acta* **2009**, *54*, 1932.
9. Lawrence, N. S.; Pagels, M.; Meredith, A.; Jones, T. G. L.; Hall, C. E.; Pickles, C. S. J.; Godfried, H. P.; Banks, C. E.; Compton, R. G.; Jiang, L. *Talanta* **2006**, *69*, 829.
10. Yang, C. *Microchim. Acta* **2004**, *148*, 87.
11. Del Mar Cordero-Rando, M.; Barea-Zamora, M.; Barbera-Salvador, J. M.; Naranjo-Rodriguez, I.; Munoz-Leyva, J. A.; De Cisneros, J. L. H.-H. *Microchim. Acta* **1999**, *132*, 7.
12. Danhel, A.; Shiu, K. K.; Yosypchuk, B.; Barek, J.; Peckova, K.; Vyskocil, V. *Electroanalysis* **2009**, *21*, 303.
13. Hutton, E. A.; Ogorevc, B.; Smyth, M. R. *Electroanalysis* **2004**, *16*, 1616.
14. Campo Dallórto, V.; Danilowicz, C.; Sobral, S.; Lo Balbo, A.; Rezzano, I. *Anal. Chim. Acta* **1996**, *336*, 195.
15. Guo, S.; Wang, E. *Anal. Chim. Acta* **2007**, *598*, 181.
16. Sheridan, E.; Hjelm, J.; Forster, R. J. *J. Electroanal. Chem.* **2007**, *698*, 1.
17. Wang, J.; Wang, L.; Di, J.; Tu, Y. *Talanta* **2009**, *77*, 1454.
18. Liu, Z.; Du, J.; Qiu, C.; Huang, L.; Ma, H.; Shen, D.; Ding, Y. *Electrochem. Commun.* **2009**, *11*, 1365.
19. Tsai, M.-C.; Chen, P.-Y. *Talanta* **2008**, *76*, 533.
20. Zhou, N.; Wang, J.; Chen, T.; Yu, Z.; Li, G. *Anal. Chem.* **2006**, *78*, 5227.